AIP | Journal of Applied Physics

Light-induced V oc increase and decrease in high-efficiency amorphous silicon solar cells

M. Stuckelberger, Y. Riesen, M. Despeisse, J.-W. Schüttauf, F.-J. Haug, and C. Ballif

Citation: Journal of Applied Physics **116**, 094503 (2014); doi: 10.1063/1.4894457
View online: http://dx.doi.org/10.1063/1.4894457
View Table of Contents: http://scitation.aip.org/content/aip/journal/jap/116/9?ver=pdfcov
Published by the AIP Publishing

Light-induced V_{oc} increase and decrease in high-efficiency amorphous silicon solar cells

M. Stuckelberger,[a] Y. Riesen, M. Despeisse, J.-W. Schüttauf, F.-J. Haug, and C. Ballif
Ecole Polytechnique Fédérale de Lausanne (EPFL), Institute of Microengineering (IMT), Photovoltaics and Thin-Film Electronics Laboratory, Rue de la Maladière 71, CH-2000 Neuchâtel, Switzerland

(Received 2 July 2014; accepted 21 August 2014; published online 4 September 2014)

High-efficiency amorphous silicon (*a*-Si:H) solar cells were deposited with different thicknesses of the *p*-type amorphous silicon carbide layer on substrates of varying roughness. We observed a light-induced open-circuit voltage (V_{oc}) increase upon light soaking for thin p-layers, but a decrease for thick p-layers. Further, the V_{oc} increase is enhanced with increasing substrate roughness. After correction of the *p*-layer thickness for the increased surface area of rough substrates, we can exclude varying the effective *p*-layer thickness as the cause of the substrate roughness dependence. Instead, we explain the observations by an increase of the dangling-bond density in both the *p*-layer—causing a V_{oc} increase—and in the intrinsic absorber layer, causing a V_{oc} decrease. We present a mechanism for the light-induced increase and decrease, justified by the investigation of light-induced changes of the *p*-layer and supported by Advanced Semiconductor Analysis simulation. We conclude that a shift of the electron quasi-Fermi level towards the conduction band is the reason for the observed V_{oc} enhancements, and poor amorphous silicon quality on rough substrates enhances this effect.
 [http://dx.doi.org/10.1063/1.4894457]

I. INTRODUCTION

Light-induced changes of hydrogenated amorphous silicon (*a*-Si:H) have been widely discussed in the literature since the discovery of the Staebler-Wronski effect[1] (SWE) in 1977. Most of these studies refer to light-induced degradation (LID) of the intrinsic (*i*) absorber layer.[2–7] Not only do *a*-Si:H layers suffer from LID, but amorphous silicon alloys such as amorphous silicon carbide (*a*-SiC:H) and amorphous silicon oxide (*a*-SiO:H) also degrade.[8–10] Both carbon and oxygen are often used to widen the bandgap of intrinsic or doped amorphous silicon—and there is no reason why alloys using them would not degrade when they are boron doped.

Light-induced changes of the complete device can have different origins. One of them is the SWE of intrinsic *a*-Si:H layers, but also ZnO, which is often used as a transparent conductive oxide (TCO) as the front and back electrodes of solar cells, degrades during light soaking.[11] Also, the electrical contact between the TCO and a metallic back contact is improved by annealing that is performed typically right after solar cell deposition, but the improvement can be seen during light soaking, if the solar cell is not annealed before. (This effect can be used to report very low or even positive light-induced changes starting from low solar cell efficiencies.) In contrast to such irreversible light-induced changes, strictly speaking the SWE refers to only the part of LID that is due to a light-induced change of photo-conductivity, and that is reversible by annealing.[1] Solar cells can run through many degradation/annealing cycles during normal operation.[12–14]

The underlying reason for the SWE is still under discussion. Several models[15–18] provide explanations on the atomic level with or without an active role of mobile hydrogen and hydrogen–silicon bonds. They have in common that structural defects are created by recombination of charge carriers during light soaking. These defects form electronic states near mid-gap that act as recombination centers and limit efficient charge collection.

Nearly 40 yr after the discovery of LID of *a*-Si:H, the negative impact of SWE on thin-film silicon solar cells has still not been significantly reduced, and it is questionable whether solar cells based on *a*-Si:H as the absorber will ever overcome this limitation that seems to be inherently linked to its amorphous nature.

However, LID of solar cells can have a positive effect on solar cells. In particular, the open-circuit voltage (V_{oc}) can be increased during light soaking. This effect has been reported by several research institutes,[13,19–29] however, it has never been studied thoroughly or been explained satisfyingly.

Such light-induced V_{oc} enhancement is the subject of the present study. After a short description of the experimental design in Sec. II, we show in Sec. III under which circumstances V_{oc} enhancement can occur, and we discuss light-induced changes of single layers, mainly of the *p*-type amorphous silicon carbide, *p*-(*a*-SiC:H), and the intrinsic *a*-Si:H absorber layers. Then, we discuss V_{oc} enhancement with respect to kinetics and with respect to substrate roughness dependence. Finally, in Sec. IV, we provide an explanation of the observed effects on the basis of a layer-by-layer simulation, with only light-induced defect generation as the changing parameter.

II. EXPERIMENTAL DETAILS

The main results of this study were obtained from a thickness series of the *p*-(*a*-SiC:H) layer incorporated in a high-efficiency *a*-Si:H solar cell.

[a]Electronic mail: michael.stuckelberger@epfl.ch

Figure 1 gives an overview over the structure and layer thicknesses of the solar cells deposited in the *p-i-n* (superstrate) configuration on 0.5-mm-thick Schott AF 32 glass substrates. Single layers were co-deposited on 250 -μm-thick double-side-polished intrinsic (100) crystalline silicon (*c*-Si) wafers for Fourier transform infrared spectroscopy (FTIR) measurements, and on 0.5-mm-thick Schott AF 32 glass substrates for all other measurements. Details about layer characterization are given elsewhere.[30,31]

For the front electrodes, boron-doped ZnO (ZnO:B) was deposited by low-pressure chemical vapor deposition (LPCVD). For each *p*-(*a*-SiC:H) thickness, the solar cells were co-deposited on four different substrates with varying roughness: Three substrates consisted of co-deposited, 2.3-μm-thick ZnO:B on glass. On one of these, as-deposited ZnO:B was used (Z2.3 0′); on the two others, the ZnO:B was treated for 7 or 20 min with an argon plasma to modify the surface texture from its initial V-shape into a smoother U-shape (Z2.3 7′ and Z2.3 20′, respectively). This leads to less shunting but also less light scattering.[32] The fourth substrate was a flat reference with smoothly grown, 0.8-μm-thick LPCVD ZnO:B, treated for 4 min with an argon plasma (Smooth 4′).[33,34]

We deposited a *p*-type microcrystalline silicon-oxide layer, denoted by *p*-(μc-SiO:H), in direct contact with the front ZnO for good electrical contact, transparency, and shunt quenching.[35,36] For a strong electric field, a *p*-(*a*-SiC:H) layer with a wide bandgap was deposited after the *p*-(μc-SiO:H) layer. The thickness of this layer was varied between 0 (no deposition) and about 20 nm. For the solar cells without a *p*-(*a*-SiC:H) layer, the same process flow was kept (gas flows, heating times, etc.), but without igniting the plasma. Details of this layer are discussed elsewhere.[31] Between the *p*-type layers and the intrinsic absorber layer, we added a wide-bandgap *a*-SiO:H layer.[37] The *a*-Si:H absorber layer has a low Tauc-Lorentz bandgap[38,39] of 1.66 eV. An *n*-type amorphous silicon layer, *n*–(*a*-Si:H), and an *n*-type microcrystalline silicon-oxide layer, *n*–(μc-SiO:H), were deposited after the absorber layer to complete the *p-i-n* junction. The back electrode consists of 2.3–μm-thick LPCVD-grown ZnO:B. For each substrate, an array of 12 cells, each 0.25 cm^2 in size, was defined by a combination of wet and dry etching.

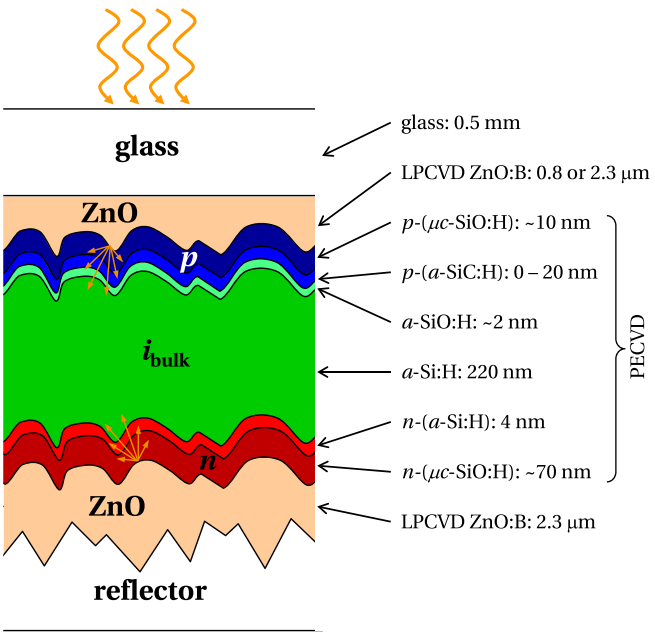

FIG. 1. Solar cell structure used for the *p*-(*a*-SiC:H) thickness series on four different substrates.

All silicon layers were deposited by plasma-enhanced chemical vapor deposition (PECVD) in a cluster tool (Octopus I) from INDEOtec SA[40] with dedicated chambers for *p*-type, *n*-type, and *i*-layers. All doped layers and the *a*-SiO:H buffer layer were deposited at 200 °C and 40.68 MHz. The absorber layer was deposited at 230 °C and 13.56 MHz. More details about individual layers, the reactor, and gas precursors can be found elsewhere.[30]

We measured current-voltage ($I(V)$) characteristics under a four-lamp (three halogen, one xenon) solar simulator from Wacom (class AAA) under standard conditions (AM1.5g, 1000 W/m^2, 25 °C).[41,42] The current was determined from external quantum efficiency (*EQE*) measurements, taken with a system built in-house. Back reflectors made from of polytetrafluoroethylene (PTFE) were used for current measurements.

Before light soaking the solar cells, each substrate was cut into two. Eight of the 12 solar cells were light soaked in a solar simulator from Solaronix (class AAA) for 1000 h at 50 °C under 500 W/m^2 of AM1.5g light. The solar cell in the center of the substrate that performed best after light soaking was used for the analysis in Secs. III B and III D. The other four solar cells were contacted by ultrasonic soldering and light soaked with in-situ measurement of the LID kinetics. These measurements were performed with three-sun-equivalent illumination for one day at 50 °C. A dedicated solar simulator[43] fully based on light-emitting diodes (LEDs) and built in-house was used for these measurements, which are presented in Sec. III C.

The simulations presented in Sec. IV were performed using the Advanced Semiconductor Analysis (ASA) software package (version 6).[44,45] The input parameters for the simulation are given in the Appendix, and relevant choices are discussed in Sec. IV.

III. EXPERIMENTAL RESULTS AND DISCUSSION

A. Window layer changes by light soaking

First, we briefly discuss possible light-induced changes of the window layers, i.e., of the ZnO and of the *p*-type layers.

From the literature,[11,46] we know that LPCVD ZnO degrades during light soaking. However, these effects (enhancement of conductivity and reduction of transparency) are independent of the *p*-(*a*-SiC:H) thickness that we investigate in this study and thus always affect the short-circuit current density (J_{sc}) and the fill factor (*FF*) the same.

We carefully investigated possible light-induced changes of the *p*-(*a*-SiC:H) layer by different means; however, we did not detect any change in absorption from photo-spectrometry and photothermal deflection spectroscopy (PDS),[47,48] optical properties (bandgap and refractive indices) from ellipsometry, electrical properties (activation

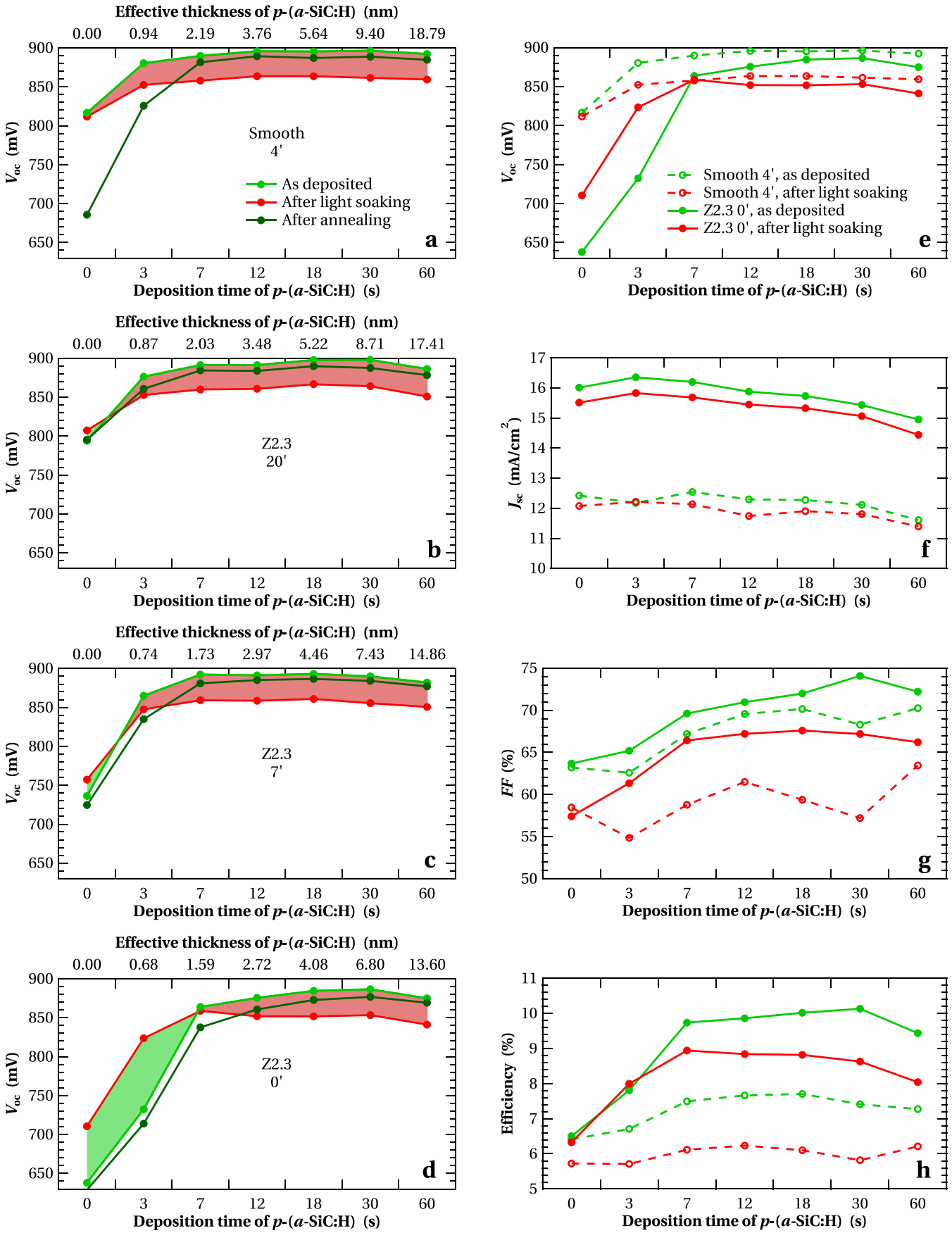

FIG. 2. (a)-(d): Open-circuit voltage in the initial state (as deposited), after light soaking, and after annealing for a *p*-(*a*-SiC:H) thickness series in *a*-Si:H solar cells on substrates with increasing roughness from a to d. The shading represents gain (green) and loss (red) of V_{oc} during light soaking. (e)-(h): V_{oc}, short-circuit current J_{sc}, fill factor *FF*, and conversion efficiency of the same series for the smoothest and roughest substrates in the initial state and after light soaking.

energy) from temperature-dependent dark conductivity measurements (confirmed independently),[49] and silicon–hydrogen bond environment from FTIR measurements.[50] These measurements were presented elsewhere,[31,51] together with measurements indicating that the *p*-(*a*-SiC:H) layer is electronically dead. This means electron–hole pairs that are created in this layer do not contribute to current.

In the following, we will take defect generation in the *p*-(*a*-SiC:H) layer into account for the explanation of light-induced V_{oc} increase, although we could not see such a change of defect states by PDS measurements. We suppose that the additional absorption due to the light-induced defects is hidden in our measurements in the strong absorption of states that are not light-induced defects (the absorption of this *p*-(*a*-SiC:H) layer at 1.2 eV is about 100 times stronger than for intrinsic *a*-Si:H material): the expected absorption change by light-induced defects is much smaller than the measurement error. Measurements of higher precision could eventually clarify this.

B. Solar cell changes by light soaking

In this section, we focus on light-induced changes of solar cells, especially of their V_{oc}. Figures 2(a)–2(d) show the V_{oc} in the initial state, after light soaking, and after annealing for a *p*-(*a*-SiC:H) layer thickness series on four substrates with increasing substrate roughness. We note:

(i) V_{oc} generally increases with increasing *p*-(*a*-SiC:H)-layer thickness; the effect is strong for thin layers and saturates with thicker layers.
(ii) For thick *p*-(*a*-SiC:H) layers (>10 nm), V_{oc} decreases slightly with increasing layer thickness.
(iii) For thin *p*-(*a*-SiC:H)-layers, V_{oc} increases during light soaking.
(iv) For thick *p*-(*a*-SiC:H) layers, V_{oc} decreases during light soaking.
(v) Annealing after light soaking returns V_{oc} to the initial state, i.e., V_{oc} increases for thick and decreases for thin *p*-(*a*-SiC:H) layers. An exception is the flattest substrate. From previous studies[11] we know that this kind of ZnO reacts strongly to light soaking and annealing. Therefore, we suppose that the different behavior of cells grown on this substrate is related to the ZnO and not to the *p*-(*a*-SiC:H) layer.
(vi) Rough substrates need a thicker effective *p*-(*a*-SiC:H) layer than smooth substrates for similar V_{oc}. However, the maximum V_{oc} of cells on rough substrates is lower than on smooth substrates.
(vii) The (reversible) increase of V_{oc} for thin, and decrease of V_{oc} for thick, *p*-(*a*-SiC:H) layers with light soaking is substrate-roughness dependent: The critical *p*-(*a*-SiC:H)-layer thickness at which V_{oc} does not change by light soaking is larger for rougher substrates.

We will provide explanations for each of these observations in the remaining parts of Sec. III. Note that these observations are not the result of a single experiment. Rather, we have reproduced these trends for *p*-(*a*-SiC:H) thickness series in three different reactors ranging in size and type from laboratory to industrial using different recipes, with and without oxide in the microcrystalline silicon layers. Further, another laboratory has independently confirmed the results.[49] The observation that V_{oc} is hardly changing in Fig. 2(a) for no *p*-(*a*-SiC:H) layer is not systematic: in some cases, we have observed an increasing V_{oc} even for the smoothest substrate without a *p*-(*a*-SiC:H) layer.

Figures 2(e)–2(h) show the solar cell parameters V_{oc}, J_{sc}, *FF*, and conversion efficiency as a function of the *p*-(*a*-SiC:H) layer thickness for the smoothest (smooth 4′) and the roughest (Z2.3 0′) substrates.

In Fig. 2(f), we see that J_{sc} first increases with *p*-(*a*-SiC:H)-layer thickness. This is due to improved charge collection, which overcompensates for the fact that the *p*-(*a*-SiC:H) layer leads to parasitic absorption. For thicker layers, the current decreases due to the parasitic absorption by the electronically dead *p*-(*a*-SiC:H) layer. For very thick layers, the light intensity being absorbed in the *i*-layer is sufficiently reduced that quasi-Fermi-level splitting and hence V_{oc} get smaller. This explains observation (ii). Note that the current is about 30% higher for the rough substrate as compared to the smooth substrate due to better light scattering.

In Fig. 2(g), we see that the *FF* generally increases with *p*-(*a*-SiC:H)-layer thickness. Obviously, the better charge collection overcompensates for the higher series resistance introduced by the *p*-(*a*-SiC:H) layer. On rough substrates, the *FF* is higher than on the smooth substrate. In fact, the smooth substrate is more resistive, which limits the *FF*, and the substrate itself degrades more during light soaking.

The combined changes of V_{oc}, J_{sc}, and *FF* are shown in the conversion efficiency in Fig. 2(h). For the smooth substrate, the efficiency does not depend significantly on the *p*-(*a*-SiC:H)-layer thickness; the stronger degradation of V_{oc} and *FF* for thicker layers offsets the initially higher V_{oc}. This is not the case for rougher substrates, where in some cases even a light-induced improvement caused by the V_{oc} increase was observed for thin *p*-(*a*-SiC:H) layers. For thicker *p*-(*a*-SiC:H) layers, LID is more important due to stronger degradation of V_{oc} and *FF*. This leads to a shift in optimum *p*-(*a*-SiC:H)-layer thickness from about 7 nm in the initial state, to about 1.6 nm in the degraded state.

These findings impact thin-film solar cell development, especially on rough substrates, which are required for good light trapping.[52] The positive news, that V_{oc} increases with light soaking for thin *p*-(*a*-SiC:H) layers, leads to lower optimum thickness after light soaking, which is beneficial because of lower parasitic absorption, hence higher current densities. This also reinforces the observation that solar cell optimization needs to be performed in the light-soaked state.

C. Solar cell degradation kinetics

Figure 3 shows the kinetics of the light-induced V_{oc} changes for the solar cells on the rough Z2.3 0′ substrates, during one day of light soaking under three-sun-equivalent light intensity. The substrate temperature and light intensity were stable within a few permill (cf. top of Figs. 3 and 4); the scattering in the V_{oc} measurements is caused mainly by noisy *I*(*V*) measurements. The V_{oc} increase for thin and the decrease for thick *p*-(*a*-SiC:H) layers are confirmed by these

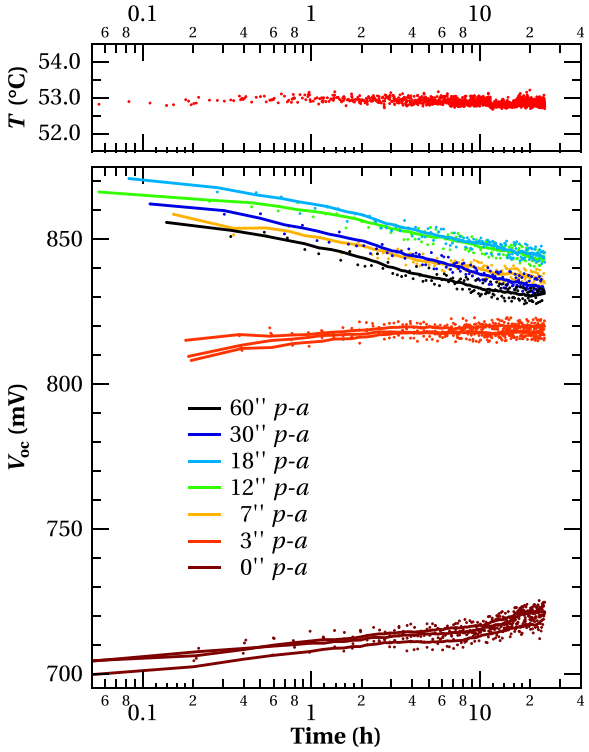

FIG. 3. Kinetics of light-induced V_{oc} changes over one day under three-sun-equivalent light intensity for cells with different p-(a-SiC:H) layer thicknesses. For thin p-(a-SiC:H) layers, measurements of three different cells are shown to demonstrate reproducibility. Lines are the smoothed measurements that are shown as spots. On top, the substrate temperature is given.

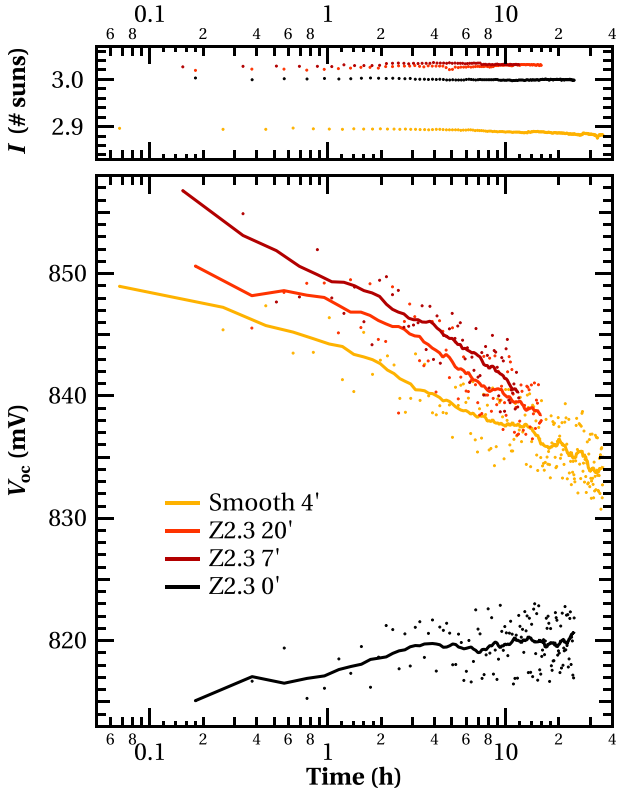

FIG. 4. Kinetics of light-induced V_{oc} changes for solar cells co-deposited on substrates with different roughnesses. Lines are smoothed measurements that are shown as spots. On top, the light intensity in number of sun equivalents is given.

light-soaking experiments. Also, the optimum layer thickness with the highest V_{oc} is the same (18 s of deposition time in the initial state, thinner layers after light soaking).

Note that all curves are linear in a semi-logarithmic scale, which means that these light-induced changes follow logarithmic laws. A single slope is observed for each curve. This observation is in contrast to recent degradation measurements[53] that show a change in kinetics after about 10 h from fast to slower degradation. The authors attribute their observation to nano-structure. For denser absorber layers with fewer voids, the fast degradation was less pronounced, which could explain why we did not observe it for our optimized absorber layer.[54]

Figure 4 shows the substrate dependence of the degradation kinetics for all four substrates of the solar cells with 3 s of p-(a-SiC:H) deposition. For this layer thickness, the V_{oc} still increases for the roughest substrate, while it decreases for the other substrates, for which the p-(a-SiC:H) is thicker than the critical thickness as indicated in Figs. 2(a)–2(d) by the crossing of the curves "as deposited" and "after light soaking." Compared with the V_{oc} measurements there, the substrate order of smooth 4′/Z2.3 20′/Z2.3 7′ is the opposite here. The reason is that, for kinetics measurements, the substrates could not be light soaked at once and the light intensity was slightly lower for smooth substrates than for rough substrates.

D. Substrate-dependent effective *p*-(*a*-SiC:H)-layer thickness

In this section, we investigate whether the strong substrate dependence of light-induced V_{oc} changes seen in Fig. 2 could come from different effective p-(a-SiC:H) layer thicknesses altering the substrate roughnesses.

Therefore, atomic force microscopy (AFM) images of the substrates, shown in Fig. 5, were taken. The main results are summarized in Table I.

Histograms of these measurements are shown in Fig. 6 with the flattened surfaces (s_{flat}) indicated. It is calculated from the effective substrate surface divided by the projected surface on the plane. We see from these calculations that the effective surface of the roughest substrate is less than 1.4 times larger than that of the smoothest substrate.

Let us assume that the total deposited volume of p-(a-SiC:H) material is the same on each substrate. This assumption can be justified by the facts that surface chemistry of all substrates is the same and the deposition rate is limited by the amount of dissociated layer precursors in the plasma. Therefore, we estimate the effective p-(a-SiC:H) layer thickness in the solar cells as $d_{eff} = r_{eff} \cdot t_{depo}$ with $r_{eff} = \frac{r_{nom}}{s_{flat}}$. Here, r_{eff} is the effective deposition rate, t_{depo} the deposition time, and $r_{nom} = 3.41$ Å/s the nominal deposition rate of the p-(a-SiC:H) layer on flat glass, determined from ellipsometry and transmittance measurements. These effective thicknesses are given as top axes in Figs. 2(a)–2(d).

Comparing the effective p-(a-SiC:H) layer thicknesses on different substrates, we see that they are less then 1.4 times thicker on the smoothest as compared to the roughest substrate. This cannot sufficiently explain the substrate roughness dependence of V_{oc} in Figs. 2(a)–2(d), where the shift of the critical p-(a-SiC:H) thickness is much larger than

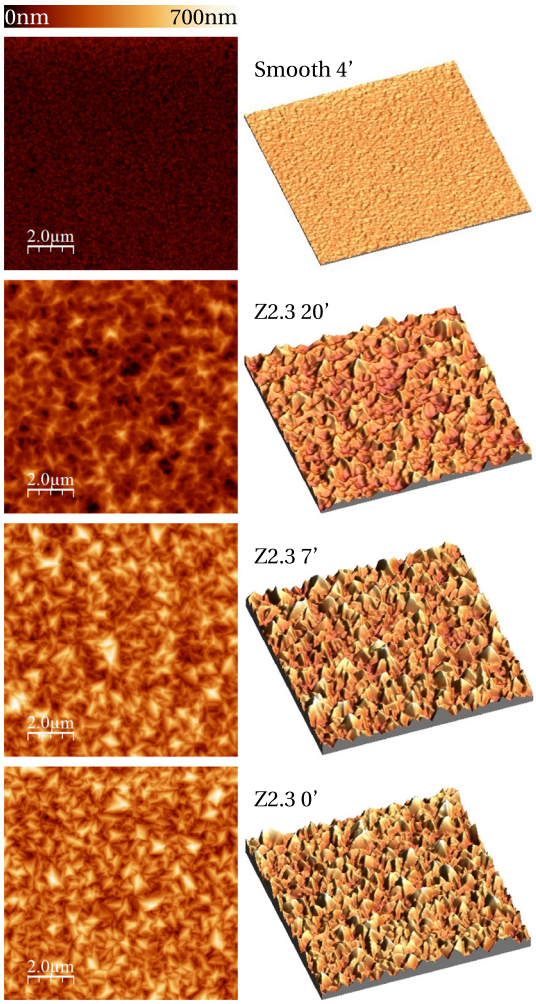

FIG. 5. AFM images of the substrates used for the solar cells presented in Fig. 2. The measurement range was 10 μm × 10 μm. Left: top-view, keeping the color scale constant for all images. Right: 3-dimensional view, keeping the height scales constant (height is double proportional to the planar dimensions). These measurements were taken by M. Leboeuf from CSEM Neuchâtel, Switzerland.

a factor 1.4. So, we have at least two effects for this shift—in Sec. IV E we will present an additional explanation.

IV. SIMULATION

All input parameters for the simulation of the *p*-(*a*-SiC:H) thickness series by the latest version of ASA are given in the Appendix. Layer measurements, where they were available, were used for input parameters in the simulations.

The *p*-(*a*-SiC:H) thickness was varied—as in the experiment—from 0 to 20 nm. In order to keep the model as simple as possible, the defect density was assumed to be constant in depth for all layers, however, on a different level for each layer, similar to earlier simulation studies.[55] To simulate the LID, the defect density of the intrinsic *a*-Si:H and *a*-SiO:H layers was increased by a factor of 5, and the defect density of the *p*-(*a*-SiC:H) layers was increased by a factor of 10, as reported in the Secs. IV A–IV F. We would like to stress that all other parameters were not modified for simulating LID, especially not activation energies E_{act}, bandgap (E_g), or other parameters linked to layer properties that were found to be stable.[31]

TABLE I. ZnO substrate parameters extracted from AFM measurements. RMS stands for root-mean square, s_{flat} for the flattened surface.

Substrate	RMS roughness	Average height	s_{flat}
Smooth 4′	14.0 nm	51 nm	1.09 cm^2/cm^2
Z2.3 20′	68.9 nm	168 nm	1.17 cm^2/cm^2
Z2.3 7′	95.3 nm	289 nm	1.38 cm^2/cm^2
Z2.3 0′	92.7 nm	300 nm	1.50 cm^2/cm^2

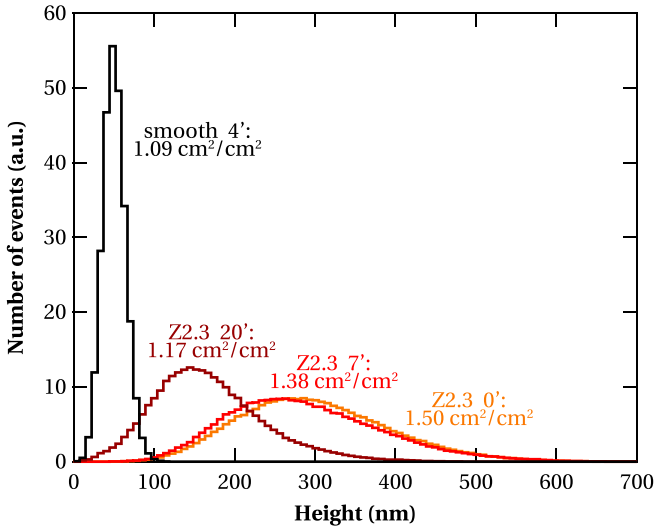

FIG. 6. Histograms of the AFM measurements of the substrates used, with the flattened surface extracted for each substrate.

A. ASA simulated light-induced V_{oc} changes

The choices of the dangling-bond density for the initial and degraded states are reported in Table II. Here, the data sets *p*-(*a*-SiC:H) and *a*-Si:H (A) have been used.

Figure 7 shows the results of these simulations. Starting from the initial state of the solar cells (p_{ini}, i_{ini}), the V_{oc} decreases with increasing dangling-bond density N_{db} in the *i*-layers (p_{ini}, i_{deg}), for all *p*-(*a*-SiC:H) layer thicknesses.

However, if the N_{db} in the *p*-(*a*-SiC:H) layer is modified (from (p_{ini}, i_{ini}) to (p_{deg}, i_{ini}), an increase of V_{oc} is observed for all *p*-(*a*-SiC:H) layer thicknesses. This is on first view surprising, as this layer is considered to be an electronically dead layer, and it seems counterintuitive that a solar cell can be improved by adding defects. In Subsection IV B, the underlying mechanism will be detailed.

Only when the N_{db} increases in both the *p*-(*a*-SiC:H) and the *i*-layers are combined does the simulation reproduce

TABLE II. Dangling-bond densities of the *p*-(*a*-SiC:H) and intrinsic *a*-Si:H layer, for ASA input of the solar cell simulation in the initial and degraded states.

Layer	N_{db}^{ini}	N_{db}^{deg}
p-(*a*-SiC:H)	1.0×10^{19} cm^{-3}	1.0×10^{20} cm^{-3}
a-Si:H (A)	5.0×10^{16} cm^{-3}	1.0×10^{17} cm^{-3}
a-Si:H (B)	1.5×10^{17} cm^{-3}	2.0×10^{17} cm^{-3}
a-Si:H (C)	1.5×10^{17} cm^{-3}	3.0×10^{17} cm^{-3}

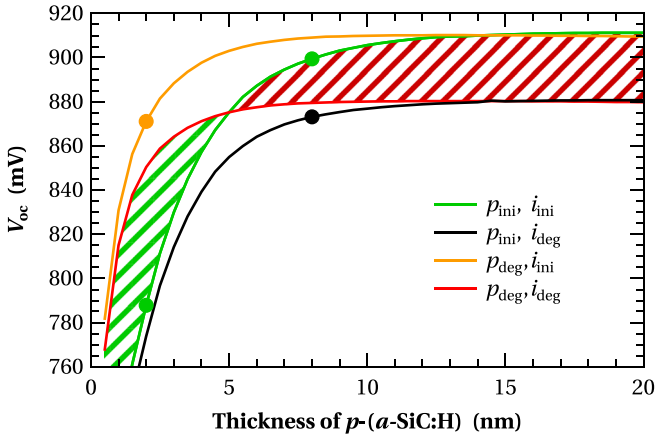

FIG. 7. Simulated V_{oc} of a *p*-(*a*-SiC:H) thickness series. Four cases are shown, differentiating between the initial and degraded states of the *p*-(*a*-SiC:H) and *a*-Si:H layers. The markers indicate solar cells that are discussed in greater detail later.

the characteristic light-induced changes of V_{oc}, i.e., an increase for thin, and a decrease for thick, *p*-(*a*-SiC:H) layers that we observed experimentally, with a critical layer thickness for which V_{oc} does not change during light-soaking.

Note that these findings are not the result of a unique choice of simulation parameters. In fact, changing the input parameters such as E_{act}, E_g, or N_{db} within a reasonable range changes only the level of V_{oc} and the critical *p*-(*a*-SiC:H)-layer thickness, but not the general trend of an increasing V_{oc} for thin and a decreasing V_{oc} for thick *p*-(*a*-SiC:H) layers. Depending on the choice of the input parameters, "thin" can mean 0 to more than 20 nm, and "thick" denotes thicknesses above the critical *p*-(*a*-SiC:H)-layer thickness.

B. The physics behind the V_{oc} increase with light soaking

We focus here on solar cells with a 2-nm-thick *p*-(*a*-SiC:H) layer and compare the two cases (p_{ini}, i_{ini}) and (p_{deg}, i_{ini}), marked in Fig. 7, to understand the V_{oc} enhancement.

Under open-circuit condition, the net current at the contacts is of course 0, all electron–hole pairs recombine somewhere in the solar cell, and the absolute values of the electron and the hole currents (both directional towards the

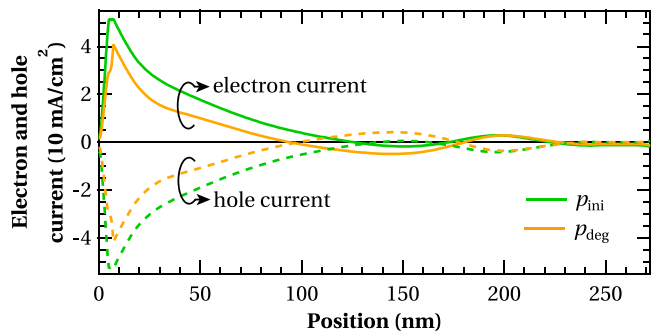

FIG. 8. Electron and hole current as a function of the position in the solar cell, where 0 marks the front ZnO/*p* interface and 272 nm the back *n*/ZnO interface. The two curves correspond to the solar cells with 2-nm-thick *p*-(*a*-SiC:H) layers indicated in Fig. 7.

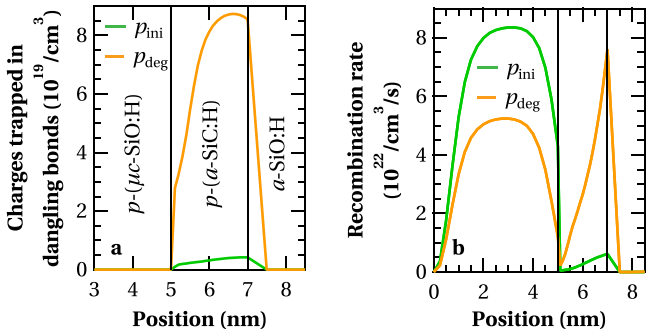

FIG. 9. Density of charges that are trapped in the dangling bonds in the *p*-(*a*-SiC:H) layer (a), and the rate of electron–hole recombinations in the *p*-(*μc*-SiO:H) and the *p*-(*a*-SiC:H) layer (b).

p-layers at most positions in the solar cell) are the same, as shown in Fig. 8.

We see there that the currents are lower for a degraded *p*-(*a*-SiC:H) layer as compared to its initial state. This is related to the increase of N_{db} which leads to an increase in the charges that are trapped in the *p*-(*a*-SiC:H) layer, and as this layer is *p*-type doped, the trapped charges are positive (see Fig. 9(a)). Vertical black lines represent here and in following figures the simulated interfaces between layers as tabulated in Table III.

Figure 9(b) shows that the increased N_{db} in the *p*-(*a*-SiC:H) layer leads to an increased recombination there. Here, only the recombination increase due to the increased N_{db} is taken into account, but not the increase of the capture cross section, when the dangling bonds are charged, which would even enhance this effect.[8,55–57]

As not many electron–hole pairs are generated in the *p*-type layers, the increased recombination in the *p*-(*a*-SiC:H) layer must lead to a decrease in recombination in the adjacent *p*-(*μc*-SiO:H) layer. However, since recombination decreases there more than it increases in the *p*-(*a*-SiC:H) layer, the total recombination in *p*-layers is reduced, but it is enhanced in the *i*-layers.

With increased N_{db} and recombination in the *p*-(*a*-SiC:H) layer, the mobility-lifetime product ($\mu\tau$) decreases, and hence the series resistance of that layer increases for charge carriers diffusing from the *i*-layers through the *p*-(*a*-SiC:H) layer and into the *p*-(*μc*-SiO:H) layer. These two effects reduce the recombination rate in the *p*-(*μc*-SiO:H) layer, and lead therefore to a reduced concentration of free electrons as shown in Fig. 10(a).

If there are fewer free electrons in the *p*-(*μc*-SiO:H) layer, the occupation probability of the states around the electron quasi-Fermi level (E_F^n) is reduced and E_F^n shifts towards mid-gap. Hence, the (positive) space charge

TABLE III. Positions of the layer interfaces in the ASA simulation for understanding the V_{oc} increase.

Layer 1	Layer 2	Position
p-(*μc*-SiO:H)	*p*-(*a*-SiC:H)	5 nm
p-(*a*-SiC:H)	*a*-SiO:H	7 nm
a-SiO:H	*a*-Si:H	17 nm

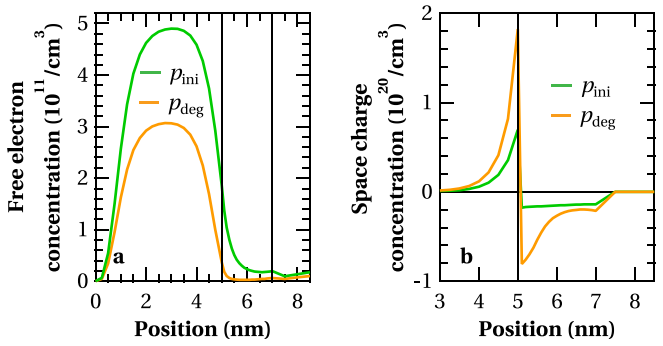

FIG. 10. Free-electron concentration in the p-(μc-SiO:H) and the p-(a-SiC:H) layer (a), and space charge concentration at the p-(μc-SiO:H)/ p-(a-SiC:H) interface that is responsible for V_{oc} enhancement with light soaking.

concentration is increased (see Fig. 10(b)), and the electrons pushed out of the p-(μc-SiO:H) layer populate the p-(a-SiC:H) layer, where the (negative) space charge concentration increases. As an alternative picture, one can imagine a p^+/p interface (the activation energies of p-(μc-SiO:H) and p-(a-SiC:H) are 0.1 and 0.4 eV) where the free-electron concentration in the p^+ layer is reduced, and hence the doping efficiency is increased.

Finally, the increased negative space charge concentration in the p-(a-SiC:H) layer shifts E_F^n there towards the conduction band edge, enhancing the quasi-Fermi-level splitting and thus the V_{oc}, as shown in the band diagram of the p-layers in Fig. 11. This mechanism explains observation (iii).

C. The physics behind the V_{oc} decrease with light soaking

Here, we focus on solar cells with an 8-nm-thick p-(a-SiC:H) layer, where a light-induced V_{oc} decrease is observed. All other simulation parameters are the same as before. Now,

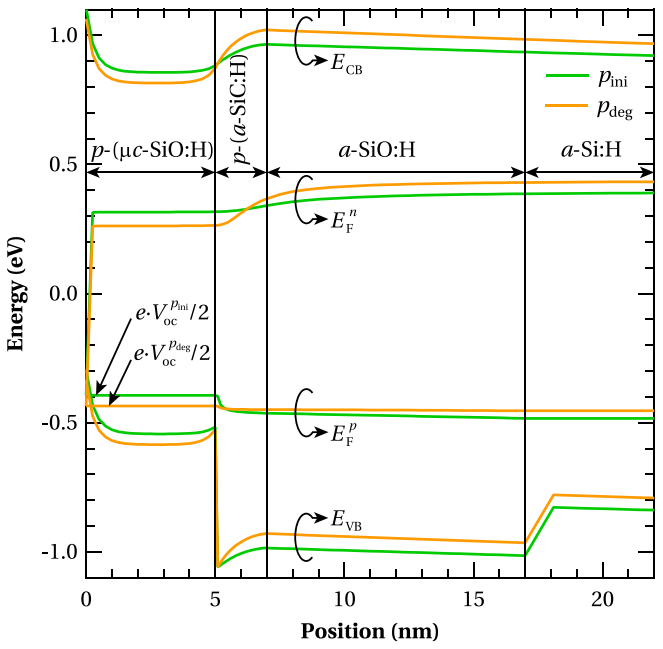

FIG. 11. Band diagram of the p-i interface of a-Si:H solar cells with a 2-nm-thick p-(a-SiC:H) layer that explains the experimentally observed V_{oc} increase in that case.

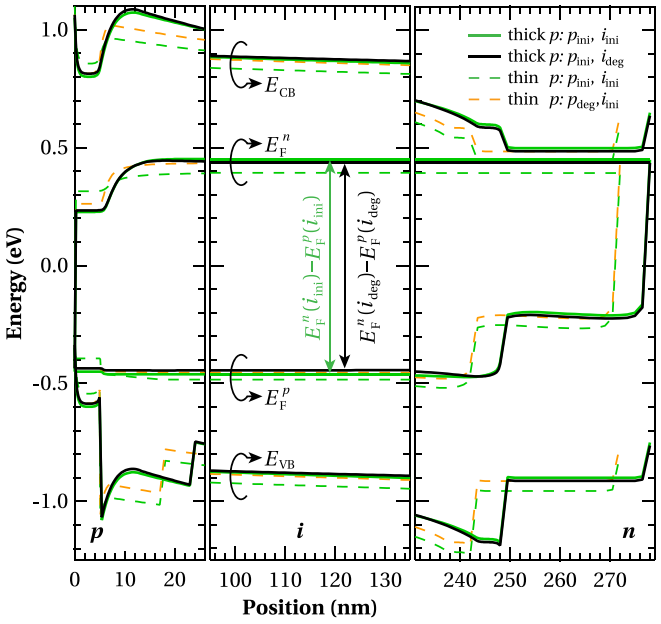

FIG. 12. Band diagram of a-Si:H solar cells with an 8-nm-thick p-(a-SiC:H) layer that explains the experimentally observed V_{oc} decrease in that case.

the V_{oc} decrease due to the i-layer degradation dominates the V_{oc} increase due to the p-(a-SiC:H)-layer degradation.

Figure 12 shows the band diagram for solar cells with a focus on the essential parts in the p-, i-, and n-layers. In order not to confuse the degradation effects of the p- with the i-layers, we consider here only the N_{db} increase from the initial (p_{ini}, i_{ini}) to the degraded (p_{ini}, i_{deg}) state as marked in Fig. 7. We see that the quasi-Fermi-level splitting in the i-layer decreases with the creation of electronic states in the bandgap, which leads directly to a V_{oc} decrease and explains observation (iv).

With this, we could explain the light-induced V_{oc} increase for thin, and the V_{oc} decrease for thick, p-(a-SiC:H) layers only by increasing the N_{db} in the p-(a-SiC:H) and i-layers. This corresponds exactly to the common understanding of the Staebler-Wronski effect and should therefore be reversible by annealing, which is observation (v).

In Fig. 12, the band diagrams of the cell with the 2-nm-thick p-(a-SiC:H) layers (shown in Fig. 11) are overlaid. The solar cell with the degraded p-(a-SiC:H) layer (p_{deg}, i_{ini}) has the same V_{oc} as the cell with the 8-nm-thick p-(a-SiC:H) layer in the (p_{ini}, i_{ini}) state, and the energy levels follow each other closely. This demonstrates, as suggested above, that the quasi-Fermi-level splitting in the p-(a-SiC:H) layer is larger for degraded p-(a-SiC:H) layers, and that this layer can fulfill its task as well as a thicker p-(a-SiC:H) layer in the initial state. In contrast, the thinner p-(a-SiC:H) layer in the initial state is too thin—with its lower space charge concentration—to push the E_F^n level sufficiently towards the conduction band. Thicker p-(a-SiC:H) layers are needed for a sufficiently large integrated charge concentration, which explains observation (i).

D. Generalisation of V_{oc} increase and decrease

For the experimental proof and explanations of the light-induced V_{oc} increase and decrease above, we used the

full layer stack as detailed in Fig. 1, which corresponds to a standard cell design at our institute. However, the results are not specific for this layer combination but generally valid as the following considerations show:

- *a-SiO:H buffer not necessary:* Using the same ASA simulation parameters as used above and detailed in the Appendix, but without the *a*-SiO:H buffer layer, a V_{oc} increase for thin and a V_{oc} decrease for thick *p*-(*a*-SiC:H) layers is revealed.
- *p-(μc-SiO:H) layer not necessary:* ASA simulations using the parameters described in the Appendix but without the *μc*-SiO:H layer is physically only reasonable if the interface with the front contact (previously ZnO/*p*-(*μc*-SiO:H), now ZnO/*p*-(*a*-SiC:H)) is adapted. Taking the different bandgaps of *p*-(*μc*-SiO:H) and *p*-(*a*-SiC:H) into account, we reduced the Schottky barrier at the interface with ZnO from 1.5 to 1.25 eV. This revealed also a V_{oc} increase for thin and a V_{oc} decrease for thick *p*-(*a*-SiC:H) layers, similarly to the case with *p*-(*μc*-SiO:H) layer.
- *Different band offsets possible:* One could think that the V_{oc} increase for thin and the V_{oc} decrease for thick *p*-(*a*-SiC:H) layers in the simulation is due to the chosen band-offset between the *p*-(*μc*-SiO:H) and the *p*-(*a*-SiC:H) layer (strong band-offset at the valence band, zero for the conduction band). We investigated this by modifying the electron affinities ("chi" in ASA input) from 4.0 to 4.1 eV for the *p*-(*μc*-SiO:H) and to 3.9 eV for the *p*-(*a*-SiC:H) layer, hence reducing the valence-band offset and enhancing the conduction-band offset. To observe a V_{oc} increase for thin *p*-(*a*-SiC:H) layers, it was thus necessary to decrease the bandgap of the *p*-(*μc*-Si:H) layer from 1.4 to 1.2 eV, which is still reasonable.

We see that our explanations are generally valid for different *p*-layer stacks with reasonably chosen simulation parameters. However, it seems that a strong valence band offset at the front-interface of the *p*-layer (in these simulations this is the interface ZnO/*p*-(*a*-SiC:H) or *p*-(*μc*-SiO:H)/*p*-(*a*-SiC:H)) is a general condition for a light-induced V_{oc} increase for thin and a V_{oc} decrease for thick *p*-layers.

E. Simulated substrate dependence

Porous zones in intrinsic *a*-Si:H above peaks of underlying ZnO were detected to cause a drop of V_{oc} in *a*-Si:H single-junction solar cells.[30,58] The part of the substrate dependence of V_{oc} that was not linked to a different effective *p*-(*a*-SiC:H)-layer thickness could be correlated to the roughness dependence of porous zones. Such porous zones with voids contain more defects—dangling bonds—than dense *a*-Si:H material.[17]

The ASA software package is not made for a precise simulation of the electrical behavior of solar cells with inhomogeneous absorber layers. Three-dimensional simulation would be needed for that. However, we can simulate an increased average dangling-bond density with ASA: Here, we have performed the same simulation as for Fig. 7, but with N_{db} higher by $1 \times 10^{17}\,cm^{-3}$, i.e., $1.5 \times 10^{17}\,cm^{-3}$ for the initial state and $2 \times 10^{17}\,cm^{-3}$ for the degraded state

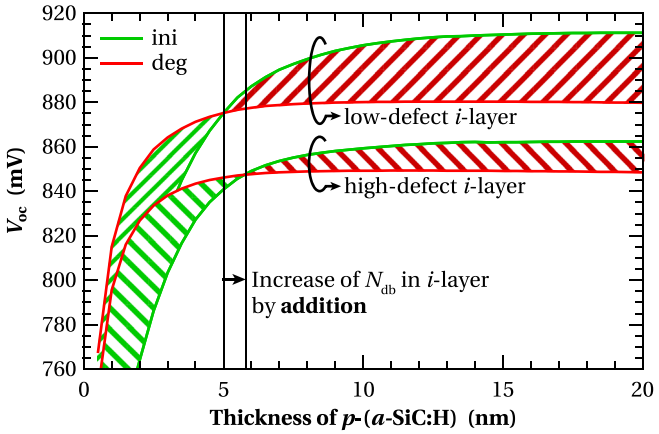

FIG. 13. Simulation of the light-induced V_{oc} changes for solar cells with low and high dangling-bond densities in the absorber layer. The dangling-bond density is increased here by addition of a constant, simulating the presence of a porous phase in the absorber layer.

(data set B in Table II). Note that we added a constant dangling-bond density, as we consider the defects from these voids to be independent from light soaking. This is in contrast to the LID, which we accounted for by multiplying N_{db} with a constant, as SWE-related N_{db} creation is proportional to the recombination rate through already existing dangling bonds.

Figure 13 shows the result of this simulation. We can clearly see that not only the V_{oc} is generally lower for more defective *i*-layers, but also that the critical *p*-(*a*-SiC:H) layer thickness, for which V_{oc} before and after degradation is the same, is shifted towards thicker *p*-(*a*-SiC:H) layers (here, from 5 to 5.8 nm). Thus, the substrate-roughness-dependent shift of the critical *p*-(*a*-SiC:H) layer thickness (observation (vii)) can be explained by a higher average defect density in the *i*-layer.

Similarly, observation (vi) can be explained: To compensate for the higher defect density in the *i*-layers and for charges trapped therein, thicker *p*-(*a*-SiC:H) layers are needed. However, V_{oc} saturates at lower values than for low-

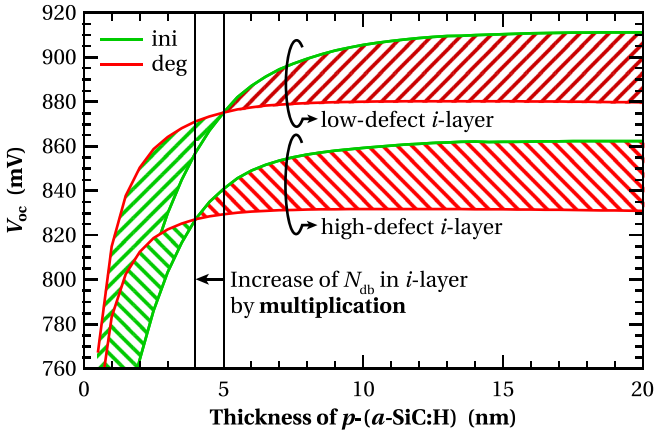

FIG. 14. Simulation of the light-induced V_{oc} changes for solar cells with low and high dangling-bond densities in the absorber layer. The dangling-bond density is increased here by multiplication with a constant, simulating poor absorber layer quality, e.g., due to a high deposition rate.

defect *i*-layers, because the quasi-Fermi-level splitting in the *i*-layer itself becomes the limiting factor.

F. Simulated *i*-layer quality dependence

Among the reported V_{oc} enhancements in the literature[3,13,19–28] (see their discussion elsewhere[51]), this effect could often be observed for absorber layers with only a few defects, but not for high-defect absorber layers. To understand this, we need another simulation, whose result is presented in Fig. 14.

The simulations with a low-defect *i*-layer are the same as those in Figs. 7 and 13. There, we *added* a constant ($+1 \times 10^{17}\,cm^{-3}$, data set B in Table II) to N_{db} to simulate porous zones in the *i*-layer. Now, we would like to simulate homogeneous *i*-layers of bad quality and do so by *multiplying* N_{db} with a constant ($\times 3$), as light-induced defect density changes are assumed to be proportional to the initial state defect density (data set C). The degradation mechanisms of the *p*-(*a*-SiC:H) and the *a*-Si:H layers remain the same between the two cases. However, it is important to note that adding a constant shifts the critical *p*-(*a*-SiC:H) layer thickness to higher values, while multiplication shifts it to lower values.

In this modeled solar cell, the case of an increasing V_{oc} for low-defect *i*-layers but decreasing V_{oc} for high-defect *i*-layers corresponds to *p*-(*a*-SiC:H) layer thicknesses between 4 and 5 nm—below the critical thickness for the low-defect *i*-layer, and above it for the high-defect *i*-layer.

V. CONCLUSIONS

Series of *a*-Si:H single-junction solar cells were deposited using a high-efficiency baseline with initial efficiencies above 10%. Varying the *p*-(*a*-SiC:H) layer thickness and the substrate roughness, we observed a light-induced V_{oc} increase for thin, and a light-induced V_{oc} decrease for thicker *p*-(*a*-SiC:H) layers. The degradation kinetic measurements showed a logarithmic light-induced degradation behavior.

By simulation of the experiments with ASA (layer-by-layer approach), we reproduced all experimentally observed effects, changing only two input parameters. We attributed the light-induced V_{oc} increase to creation of defects in the *p*-(*a*-SiC:H) layer that get charged and cause—via depletion of the *p*-(μc-SiO:H) layer—an increased negative space charge concentration in the adjacent *p*-(*a*-SiC:H) layer and thus an enhanced V_{oc}. In contrast, we attribute the V_{oc} decrease for thicker *p*-(*a*-SiC:H) layers to defect creation in the absorber layer, where the quasi-Fermi-level splitting is reduced. Simulations showed that these effects are not specific to our cell design but generally valid if the valence-band offset between the thickness-varied *p*-layer (here, the *p*-(*a*-SiC:H) layer) and the layer at the front of it (here, the *p*-(μc-SiO:H) layer) is large enough.

For optimization of thin-film silicon solar cells, the fact that V_{oc} can be enhanced by light soaking with thin *p*-(*a*-SiC:H) layers is of great importance: despite the fact that V_{oc} stays in most cases below the V_{oc} for cells with thicker *p*-(*a*-SiC:H) layers, the efficiency can be higher (especially in multi-junction solar cells) due to less parasitic absorption.

ACKNOWLEDGMENTS

We acknowledge A. Billet, L. Egger, and M. Carlberg for taking part of the solar cell measurements, N. Wyrsch, G. Bugnon, and T. Matsui (PVTEC in Tsukuba, Japan) for discussions, M. Leboeuf from CSEM, Neuchâtel, for the AFM measurements, and S. Solntsev and M. Zeman from TU Delft for providing us access to ASA software.

This work was supported in part by the Swiss Federal Office of Energy under Grant No. SI/500750-01, by the Competence Center Energy and Mobility, and Swisselectric Research (DURSOL project, www.dursol.ch), and by the FP7 Project "Fast Track," funded by the European Commission under Grant No. 283501.

APPENDIX: ASA SIMULATION INPUT PARAMETERS

We present here the input parameters we used for ASA simulations. Values indicated as VARIABLE are the crucial values that were varied and are discussed in detail in Sec. IV. For explanation of the parameters, we refer to the ASA manual.[59]

```
C Device structure;
layers electrical=6 front=2 back=1;
grid[1] d=5e-9 spaces=20;
grid[2] d=VARIABLE spaces=20;
grid[3] d=10.0e-9 spaces=20;
grid[4] d=220.0e-9 spaces=200;
grid[5] d=5.0e-9 spaces=20;
grid[6] d=30.0e-9 spaces=20;
grid[f.1] d=0.5e-3;
grid[f.2] d=2.00e-6;
grid[b.1] d=2.00e-6;

frontcon schottky e.bar=1.5;
backcon schottky e.bar=0.20;

C Optical properties;
optical[1] lnk.file=Lj_p-ucSi.nk;
optical[2] lnk.file=tud_p-aSiC.nk;
optical[3] lnk.file=tud_i-aSi.nk;
optical[4] lnk.file=tud_i-aSi.nk;
optical[5] lnk.file=tud_n-aSi.nk;
optical[6] lnk.file=tud_n-aSi.nk;
optical[f.1] ext.coeff=0 ref.index=1.5 incoherent;
optical[f.2] lnk.file=ZnoOz2min0.nk;
optical[b.1] lnk.file=ZnoOz2min0.nk;

C Semiconductor properties;
doping[1] e.act.acc=0.15;
doping[2] e.act.acc=0.4;
doping[5] e.act.don=0.15;
doping[6] e.act.don=0.05;

bands[1] e.mob=1.40 chi=4.0 nc=6.0E+26 nv=6.0E
  +26 epsilon=7.2;
bands[2] e.mob=1.95 chi=4.0 nc=6.0E+26 nv=6.0E
  +26 epsilon=7.2;
bands[3] e.mob=1.95 chi=4.0 nc=2.0E+26 nv=2.0E
  +26 epsilon=11.9;
```

```
bands[4] e.mob=1.76 chi=4.0 nc=2.0E+26 nv=2.0E+26 epsilon=11.9;
bands[5] e.mob=1.76 chi=4.0 nc=6.0E+26 nv=6.0E+26 epsilon=11.9;
bands[6] e.mob=1.40 chi=4.0 nc=6.0E+26 nv=6.0E+26 epsilon=11.9;

mobility[1] mu.e=10.0e-4 mu.h=1.0e-4;
mobility[2] mu.e=10.0e-4 mu.h=1.0e-4;
mobility[3] mu.e=20.0e-4 mu.h=5.0e-4;
mobility[4] mu.e=20.0e-4 mu.h=5.0e-4;
mobility[5] mu.e=10.0e-4 mu.h=1.0e-4;
mobility[6] mu.e=10.0e-4 mu.h=1.0e-4;

C Description of DOS;
vbtail[all] e.range=0.5 levels=50 c.neut=0.7e-15 c.pos=0.7e-15;
vbtail[1] n.emob=1.0e28 e.char=0.090;
vbtail[2] n.emob=1.0e28 e.char=0.090;
vbtail[3] n.emob=1.0e27 n1.emob=1.0e27 e.char=0.043 e1.char=0.043;
vbtail[4] n.emob=1.0e27 n1.emob=1.0e27 e.char=0.043 e1.char=0.043;
vbtail[5] n.emob=1.0e28 e.char=0.090;
vbtail[6] n.emob=1.0e28 e.char=0.090;

cbtail[all] e.range=0.5 levels=50 c.neut=0.7e-15 c.neg=0.7e-15;
cbtail[1] n.emob=5.0e27 e.char=0.070;
cbtail[2] n.emob=5.0e27 e.char=0.070;
cbtail[3] n.emob=2.0e27 e.char=0.030;
cbtail[4] n.emob=2.0e27 e.char=0.030;
cbtail[5] n.emob=1.0e28 e.char=0.080;
cbtail[6] n.emob=1.0e28 e.char=0.080;

dbond[all] levels=40 e.corr=0.2;
dbond[1] n=1e21 e.neut=-0.70 ce.pos=200.0e-15 ce.neut=1.0e-15 ch.neg=100.0e-15 ch.neut=1.0e-15;
dbond[2] n=VARIABLE e.neut=-0.70 ce.pos=200.0e-15 ce.neut=1.0e-15 ch.neg=100.0e-15 ch.neut=1.0e-15;
dbond[3] n=VARIABLE e.neut=-0.88 ce.pos=200.0e-15 ce.neut=1.0e-15 ch.neg=100.0e-15 ch.neut=1.0e-15;
dbond[4] n=VARIABLE e.neut=-0.88 ce.pos=200.0e-15 ce.neut=1.0e-15 ch.neg=100.0e-15 ch.neut=1.0e-15;
dbond[5] n=5e23 e.neut=-1.40 ce.pos=200.0e-15 ce.neut=1.0e-15 ch.neg=100.0e-15 ch.neut=1.0e-15;
dbond[6] n=1e21 e.neut=-1.40 ce.pos=200.0e-15 ce.neut=1.0e-15 ch.neg=100.0e-15 ch.neut=1.0e-15;

C Numerical settings;
model[all] amorphous;
model[all] external;
settings newton gummel.starts=2;
settings damp=3 max.iter=50;
settings sr.flux=1.0e16;
settings Rs=1e-4;

opticgen spectrum=am15.dat genpro3 mult=1.0;
```


[1]D. Staebler and C. Wronski, "Reversible conductivity changes in discharge-produced amorphous Si," Appl. Phys. Lett. **31**, 292–294 (1977).

[2]P. Roca i Cabarrocas, A. Fontcuberta i Morral, and Y. Poissant, "Growth and optoelectronic properties of polymorphous silicon thin films," Thin Solid Films **403–404**, 39–46 (2002).

[3]Y. Poissant, P. Chatterjee, and P. Roca i Cabarrocas, "Analysis and optimization of the performance of polymorphous silicon solar cells: Experimental characterization and computer modeling," J. Appl. Phys. **94**, 7305–7316 (2003).

[4]J. Melskens, M. Schouten, R. Santbergen, M. Fischer, R. Vasudevan, D. J. van der Vlies, R. J. V. Quax, S. G. M. Heirman, K. Jäger, V. Demontis, M. Zeman, and A. H. M. Smets, "In situ manipulation of the sub gap states in hydrogenated amorphous silicon monitored by advanced application of Fourier transform photocurrent spectroscopy," Sol. Energy Mater. Sol. Cells **129**, 70–81 (2014).

[5]M. Fehr, A. Schnegg, B. Rech, O. Astakhov, F. Finger, R. Bittl, C. Teutloff, and K. Lips, "Metastable defect formation at microvoids identified as a source of light-induced degradation in a-Si:H," Phys. Rev. Lett. **112**, 066403 (2014).

[6]T. Matsui, H. Sai, K. Saito, and M. Kondo, "High-efficiency thin-film silicon solar cells with improved light-soaking stability," Prog. Photovoltaics Res. Appl. **21**, 1363–1369 (2013).

[7]T. Matsui, H. Sai, T. Suezaki, M. Matsumoto, K. Saito, I. Yoshida, and M. Kondo, "Development of highly stable and efficient amorphous silicon based solar cells," in *Proceedings of the 28th EU PVSEC* (2013), pp. 2213–2217.

[8]*Thin-film Silicon Solar Cells*, edited by A. Shah (CRC Press, 2010).

[9]I. A. Yunaz, K. Hashizume, S. Miyajima, A. Yamada, and M. Konagai, "Fabrication of amorphous silicon carbide films using VHF-PECVD for triple-junction thin-film solar cell applications," Sol. Energy Mater. Sol. Cells **93**, 1056–1061 (2009).

[10]S. Inthisang, K. Sriprapha, S. Miyajima, A. Yamada, and M. Konagai, "Hydrogenated amorphous silicon oxide solar cells fabricated near the phase transition between amorphous and microcrystalline structures," Jpn. J. Appl. Phys., Part 1 **48**, 122402 (2009).

[11]L. Ding, M. Stuckelberger, M. Morales Masis, S. Nicolay, and C. Ballif, "Stability of the opto-electrical properties of Zinc Oxide electrodes in thin-film silicon solar cells under light soaking," (unpublished).

[12]P. Lechner, R. Geyer, A. Haslauer, and T. Roehrl, "Long-term performance of ASI tandem junction thin film solar modules," in *Proceedings of the 25th EU PVSEC* (2010), pp. 3283–3287.

[13]M. Isomura, H. Yamamoto, M. Kondo, and A. Matsuda, "The light-induced increase in open circuit voltage of amorphous silicon solar cells," in *Proceedings of the 2nd World Conference And Exhibition On Photovoltaic Solar Energy Conversion* (1998), pp. 925–928.

[14]E. M. El Mhamdi, J. Holovsky, B. Demaurex, C. Ballif, and S. De Wolf, "Is light-induced degradation of a-Si:H/c-Si interfaces reversible?," Appl. Phys. Lett. **104**, 252108 (2014).

[15]T. Shimizu, "Staebler-Wronski effect in hydrogenated amorphous silicon and related alloy films," Jpn. J. Appl. Phys., Part 1 **43**, 3257–3268 (2004).

[16]S. B. Zhang and H. M. Branz, "Hydrogen above saturation at silicon vacancies: H-pair reservoirs and metastability sites," Phys. Rev. Lett. **87**, 105503 (2001).

[17]A. Smets, W. Kessels, and M. van de Sanden, "Vacancies and voids in hydrogenated amorphous silicon," Appl. Phys. Lett. **82**, 1547–1549 (2003).

[18]A. Smets, C. Wronski, M. Zeman, and M. van de Sanden, "The Staebler-Wronski effect: New physical approaches and insights as a route to reveal its origin," Mater. Res. Soc. Symp. Proc. **1245**, 1245–A14–02 (2010).

[19]P. St'ahel, A. Hadjadj, P. Sládek, and P. Roca i Cabarrocas, "Metastability in boron doped a-Si:H and a-SiC:H materials: Correlation with solar cell parameters," in *Proceedings of the 14th EU PVSEC* (1997), pp. 640–643.

[20]P. Roca i Cabarrocas, P. Stáhel, S. Hamma, and Y. Poissant, "Stable single junction p-i-n solar cells with efficiencies approaching 10%," in *Proceedings of the 2nd World Conference and Exhibition on Photovoltaic Solar Energy Conversion* (1998), pp. 355–358.

[21]K. Lord, B. Yan, J. Yang, and S. Guha, "Light-induced increase in the open-circuit voltage of thin-film heterogeneous silicon solar cells," Appl. Phys. Lett. **79**, 3800–3802 (2001).

[22]J. Yang, K. Lord, B. Yan, A. Banerjee, and S. Guha, "Correlation of the open-circuit voltage enhancement of heterogeneous silicon solar cells and the Staebler-Wronski effect," in *Proceedings of the 29th IEEE PVSC* (2002), pp. 1094–1097.

[23]B. Yan, J. Yang, G. Yue, K. Lord, and S. Guha, "On the mechanism of light-induced open-circuit voltage increase in mixed-phase hydrogenated silicon solar cells," in Proceedings of the 3rd World Conference on Photovoltaic Solar Energy Conversion (2003).

[24]G. Yue, B. Yan, J. Yang, K. Lord, and S. Guha, "Kinetics of light-induced effects in mixed-phase hydrogenated silicon solar cells," Mater. Res. Soc. Symp. Proc. **762**, A12.2 (2003).
[25]E. Johnson, A. Abramov, Y. Soro, M. Gueunier-Farret, J. Méot, J. P. Kleider, and P. Roca i Cabarrocas, "Application of high deposition rate (9A/s) pm-Si:H to photovoltaic modules," in *Proceedings of the 23rd EU PVSEC* (2008), pp. 2339–2342.
[26]E. Johnson, F. Dadouche, M. Gueunier-Farret, J. Kleider, and P. Roca i Cabarrocas, "Open-circuit voltage increase dynamics in high and low deposition rate polymorphous silicon solar cells," Phys. Status Solidi A **207**, 691–694 (2010).
[27]T. Matsui, paper presented at MRS Spring Conference, San Francisco, 22 April 2014.
[28]B. Rech, C. Beneking, S. Wieder, and H. Wagner, "Initial and stabilized open-circuit voltage of a-Si:H solar cells: A discussion on the basis of dark I-V curves," in *Proceedings of the 14th EU PVSEC* (1997), pp. 574–577.
[29]M. Stuckelberger, paper presented at MRS Spring Conference, San Francisco, 22 April 2014.
[30]M. Stuckelberger, M. Despeisse, G. Bugnon, J.-W. Schüttauf, F.-J. Haug, and C. Ballif, "Comparison of amorphous silicon absorber materials: Light-induced degradation and solar cell efficiency," J. Appl. Phys. **114**, 154509 (2013).
[31]M. Stuckelberger, N. Almat, A. Billet, Y. Riesen, L. Egger, A. Walter, J.-W. Schüttauf, F.-J. Haug, and C. Ballif, "Properties and light-induced degradation of optimized p-type amorphous silicon-carbide layers," (unpublished).
[32]M. Python, E. Vallat-Sauvain, J. Bailat, D. Dominé, L. Fesquet, A. Shah, and C. Ballif, "Relation between substrate surface morphology and microcrystalline silicon solar cell performance," J. Non-Cryst. Solids **354**, 2258–2262 (2008).
[33]S. Nicolay, M. Benkhaira, L. Ding, J. Escarre, G. Bugnon, F. Meillaud, and C. Ballif, "Control of CVD-deposited ZnO films properties through water/DEZ ratio: Decoupling of electrode morphology and electrical characteristics," Sol. Energy Mater. Sol. Cells **105**, 46–52 (2012).
[34]L. Fanni, B. A. Aebersold, D. T. L. Alexander, L. Ding, M. Morales Masis, S. Nicolay, and C. Ballif, "c-texture versus a-texture low pressure metalorganic chemical vapor deposition ZnO films: lower resistivity despite smaller grain size," Thin Solid Films **565**, 1–6 (2014).
[35]P. Cuony, M. Marending, D. Alexander, M. Boccard, G. Bugnon, M. Despeisse, and C. Ballif, "Mixed-phase p-type silicon oxide containing silicon nanocrystals and its role in thin-film silicon solar cells," Appl. Phys. Lett. **97**, 213502 (2010).
[36]M. Despeisse, M. Boccard, G. Bugnon, P. Cuony, T. Söderström, G. Parascandolo, M. Stueckelberger, M. Charrière, L. Löfgren, C. Battaglia, S. Hänni, A. Billet, L. Ding, S. Nicolay, F. Meillaud, N. Wyrsch, and C. Ballif, "Low-conductivity doped layers for improved performance of thin film silicon solar cells on highly textured substrates," in *Proceedings of the 25th EU PVSEC* (2010), pp. 2793–2797.
[37]G. Bugnon, G. Parascandolo, S. Hänni, M. Stuckelberger, M. Charrière, M. Despeisse, F. Meillaud, and C. Ballif, "Silicon oxide buffer layer at the pi interface in amorphous and microcrystalline silicon solar cells," Sol. Energy Mater. Sol. Cells **120**, 143–150 (2014).
[38]G. Jellison and F. Modine, "Parameterization of the optical functions of amorphous materials in the interband region," Appl. Phys. Lett. **69**, 371–373 (1996).
[39]G. Jellison and F. Modine, "Erratum: "Parameterization of the optical functions of amorphous materials in the interband region" [Appl. Phys. Lett. **69**, 371 (1996)]," Appl. Phys. Lett. **69**, 2137 (1996).
[40]INDEOtec, Switzerland, last accessed July 20, 2014.
[41]IEC, "IEC (International Electrotechnical Commission) 60904-9 Ed.2: Photovoltaic devices - Part 9: Solar simulator performance requirements" (2007).
[42]IEC, "IEC (International Electrotechnical Commission) 60904-3 Ed.2: Photovoltaic devices-Part 3: Measurement principles for terrestrial photovoltaic (PV) solar devices with reference spectral irradiance data" (2006).
[43]M. Stuckelberger, B. Perruche, M. Bonnet-Eymard, Y. Riesen, M. Despeisse, F.-J. Haug, and C. Ballif, "Class AAA LED-based solar simulator for steady-state measurements and light soaking," IEEE J. Photovoltaics **4**, 1282–1287 (2014).
[44]B. E. Pieters, J. Krc, and M. Zeman, "Advanced numerical simulation tool for solar cells-ASA5," in *Proceedings of the Conference Record on 4th WCPEC* (2006), Vol. 2, pp. 1513–1516.
[45]M. Zeman, O. Isabella, S. Solntsev, and K. Jäger, "Modelling of thin-film silicon solar cells," Sol. Energy Mater. Sol. Cells **119**, 94–111 (2013).
[46]M. Stuckelberger, A. Billet, L. Ding, F.-J. Haug, and C. Ballif, "Light-induced degradation kinetics of boron-doped zinc oxide," (unpublished).
[47]A. Boccara, D. Fournier, and J. Badoz, "Thermo-optical spectroscopy: Detection by the "mirage effect,"" Appl. Phys. Lett. **36**, 130–132 (1980).
[48]J. Holovský, M. Schmid, M. Stuckelberger, M. Despeisse, C. Ballif, A. Poruba, and M. Vaněček, "Time evolution of surface defect states in hydrogenated amorphous silicon studied by photothermal and photocurrent spectroscopy and optical simulation," J. Non-Cryst. Solids **358**, 2035–2038 (2012).
[49]T. Matsui, private communication (2014).
[50]A. Smets and M. van de Sanden, "Relation of the Si-H stretching frequency to the nanostructural Si-H bulk environment," Phys. Rev. B **76**, 073202 (2007).
[51]M. Stuckelberger, "Amorphous silicon: Impact of process conditions on material properties and solar cell efficiency," Ph.D. thesis, Ecole Polytechnique Fédérale de Lausanne, Switzerland (unpublished).
[52]F. Meillaud, A. Billet, C. Battaglia, M. Boccard, G. Bugnon, P. Cuony, M. Charrière, M. Despeisse, L. Ding, J. Escarre-Palou, S. Hänni, L. Löfgren, S. Nicolay, G. Parascandolo, M. Stuckelberger, and C. Ballif, "Latest developments of high-efficiency micromorph tandem silicon solar cells implementing innovative substrate materials and improved cell design," IEEE J. Photovoltaics **2**, 236–240 (2012).
[53]M. Fischer, R. Quax, M. Zeman, and A. Smets, "Degradation kinetics of amorphous silicon solar cells processed at high pressure and its relation to the nanostructure," in Proceedings of the IEEE Photovoltaic Specialists Conference, Tampa, FL, 2013.
[54]M. Stuckelberger, A. Billet, Y. Riesen, M. Boccard, M. Despeisse, J.-W. Schüttauf, F.-J. Haug, and C. Ballif, "Comparison of amorphous silicon absorber materials: kinetics of light-induced degradation," Prog. Photovoltaics Res. Appl. (submitted).
[55]M. Stuckelberger, Y. Riesen, B. Perruche, M. Despeisse, N. Wyrsch, and C. Ballif, "Charge collection in amorphous silicon solar cells: cell analysis and simulation of high-efficiency pin devices," J. Non-Cryst. Solids **358**, 2187–2189 (2012).
[56]N. Beck, N. Wyrsch, C. Hof, and A. Shah, "Mobility lifetime product–A tool for correlating a-Si:H film properties and solar cell performances," J. Appl. Phys. **79**, 9361–9368 (1996).
[57]M. Stuckelberger, A. Shah, J. Krc, M. Despeisse, F. Meillaud, and C. Ballif, "Internal electric field and fill factor of amorphous silicon solar cells," in *Proceedings of the 35th IEEE Photovoltaic Specialists Conference* (2010), pp. 001569–001574.
[58]M. Stuckelberger, A. Billet, A. Walter, J.-W. Schüttauf, F.-J. Haug, and C. Ballif, "Impact of substrate roughness on charge collection in amorphous silicon solar cells," (unpublished).
[59]M. Zeman, J. van den Heuvel, M. Kroon, J. Willemen, B. Pieters, J. Krc, and S. Solntsev, Advanced Semiconductor Analysis (ASA), user's manual, version 6.0 (2013).